Metal supported cathodically activated graphite via self-reduction as electrocatalysts for efficient hydrogen evolution reaction

H.-Z. Yu, J. Ghilane

Metal supported cathodically activated graphite via self-reduction as electrocatalysts for efficient hydrogen evolution reaction

Hao-Zheng Yu, Jalal Ghilane*

Université Paris Cité, ITODYS, CNRS, UMR 7086, 15 rue J-A de Baïf, F-75013, Paris, France.

ABSTRACT: Surface modification is a promising approach to modulate the electrocatalyst properties for their further use in energy storage and conversion. In this work, electrochemical based approach was proposed to generate metallic particles supported graphite rod (GR). The approach is based on the cathodic activation of GR in the presence of alkali metal salts in dry organic solvent. The activated GR possess a high reducing power that was successfully employed to spontaneously reduce metallic salts in aqueous media. The surface analyses confirm the formation of metallic nanoparticles supported GR. Interestingly, the metallic nanoparticles were found to be generated onto and intercalated into the GR. Next, the generated materials were used as electrocatalyst to drive the hydrogen evolution reaction (HER). Our results demonstrate that the electrocatalytic performances depend on various parameters including the radius of the alkali metal cation and the injected charge during the electrochemical activation. The as-prepared Pt/Li-GR exhibits the best electrochemical activity and stability towards the HER. The necessary overpotential value to reach a current density of 10 $mA.cm^{-2}$ is 40 mV for the Pt/Li-GR, and almost negligible overpotential change is observed during the stability tests. In addition, the proposed approach was successfully used to generate Pd/Li-GR catalyst. More impressively, the latter displays higher HER performances when compared to other reported Pd based catalysts and comparable performance with commercial Pt/C catalyst.

Keywords: Electrochemistry, Surface modification, Electrocatalyst, Hydrogen evolution reaction.

1. Introduction

The utilization of fossil-free, renewable, and clean hydrogen resource with high gravimetric energy density is one of the best routes to decrease carbon dioxide emissions and meet the energy demand [1-4]. Hydrogen evolution reaction (HER) is an alternative and sustainable pathway to generate hydrogen in electrochemical water splitting for effective energy conversion and storage purpose [5-7]. To drive efficiently the HER and to increase its performances the use of catalyst is required. Despite their scarcity and high-cost Platinum-group metal (PGM) based catalysts are still the state-of-the-art and the most universal electrocatalysts [8-10]. Besides, transition metal and carbon-based catalysts have been developed showing a promising advance on HER catalysis [11,12]. Commonly, nanomaterials have been proved to be the ideal catalyst materials. There are numerous studies reporting various syntheses route to generate nanomaterial and/or alloys that have been successfully used to improve or uphold the catalytic performance towards the HER [13-16]. However, every coin has two sides; here the alloys and nanoparticles are no exceptions. The formation of alloy commonly involves high temperature or high pressure, or other harsh conditions and suffers from the inevitable agglomeration owed to the high surface energy of nano-size particles [17-19]. Other strategies have been successfully developed to increase the electrocatalytic performance, for a given material, based on the heteroatoms doping of metal or carbon nanocatalysts [20,21]. In general, the catalysts are synthesized using different steps to achieve the desired nanostructure and the process usually involves a high temperature treatment [22,23]. Next, the ink containing the catalyst and the polymer binder is coated on the electrode surface.

Carbon-based electrodes, including glassy carbon (GC) and graphite, are by far the most used support for hosting the nanocatalysts because of their low cost, abundance, non-toxicity, high stability, superior conductivity, and lower catalytic activity [24,25]. Recently, surface modifications of carbon support have been introduced as a promising approach to host-guest the catalyst material [26]. The hybrid catalyst displays improved catalytic performances attributed to the presence of synergetic effect between the attached layers on the carbon support and the nanomaterials catalysts [27]. As an example, polymer brush-based ionic liquid onto GC has been used as nanostructured support and template to induce Pt or Pd nanoparticles electrochemical growth [28-30]. In this work, it was reported that the 3-D nanostructure of the polymer, as well as the chemical composition (heteroatoms doping and electrostatic interactions) of the ionic layer, are the key parameters that boost the metal electrocatalytic activities.

Surface modification and especially the electrochemical assisted grafting is a general process related to the immobilization of organic layer, through oxidative or reductive processes, at the electrode surface [31]. However, a more specific electrochemical reaction has been reported to induce morphological change of

the electrode materials. The process is based on the cathodic activation of the electrode material leading to generate a new phase with a general formula [M_n^-, Cat^+] [32,33]. This process has been reported in the case of Pt, Au, ITO and C electrodes materials and different electrolytes including alkali metals, quaternary ammoniums and ionic liquids [34-38]. Thus during the electrochemical reduction of the electrode material, in dry organic electrolytic solution, electron transfer concomitant with the intercalation of the electrolyte cation occurred. The cathodic activation is less studied in the literature when compared to classical electrochemical assisted surface modification (i.e. the electrochemical grafting and the electropolymerization). Forty years ago, Besenhard investigated the electrochemical preparation of alkali metal-graphite intercalation [39]. Subsequently, Simonet et al. reported the electrochemical reduction of graphite in the presence of quaternary ammonium cation [40]. As a result, morphological change of the electrode surface has been reported with a swelling behavior due to the cation intercalation. The as-prepared graphite phase carried negative charge and hence displayed n-type like conductivity. More recently, the reducing power of the cathodically activated electrode materials has been used to induce spontaneous reduction of diazonium salt and metallic salts [38,41,42]. To date, a limited articles are reporting the investigation and application of the cathodic activation procedure.

The purpose of the present work was to investigate surface modification of carbon using the electrochemical reduction of graphite and subsequently generating metal/carbon materials. The proposed approach is simple and based on the formation of reducing carbon material through the electrochemical reduction in organic electrolytic solution using mild reducing potential. Next, the generated material (activated graphite, A-GR) was used to spontaneously reduce metallic salt and thus providing metal supported graphite material. Next, the generated material is characterized using surface analyses investigations confirming the spontaneous growth of metallic particles on and into the graphite rod. Furthermore, the electrocatalytic performances of the as-prepared materials towards HER were investigated and compared to the state of the art electrocatalyst. Interestingly, the activated graphite in the presence of lithium salt, to generate the Pt/Li-GR, exhibits the best electrochemical activity towards the HER. The necessary overpotential value to reach a current density of 10 $mA.cm^{-2}$ is only 40 mV. In addition, the proposed approach was successfully used to generate Pd/Li-GR catalyst. More impressively, the latter displays higher HER performances when compared to other reported Pd based catalysts and shows comparable performance with commercial Pt/C catalyst.

2. Experimental section

2.1. Chemicals and Materials

Potassium tetrachloroplatinate(II) (K_2PtCl_4) and sodium tetrachloropalladium(II) monohydrate (Na_2PCl_4) were supplied by Sigma-Aldrich. Bis(trifluoromethane)sulfonimide lithium salt (LiTFSI), sodium tetrafluoroborate ($NaBF_4$), and potassium tetrafluoroborate (KBF_4) supplied from Sigma-Aldrich and were used as supporting electrolytes. Commercial platinum on graphitized carbon (Pt/C, 20 wt%) were purchased from Sigma Aldrich. acetonitrile (ACN), sulphuric acid (H_2SO_4, 95%), ethanol absolute (EtOH) were purchased from VWR International, LLC. Nafion® D-520 dispersion (5 wt %) and graphite rod (GR, 3.05 mm of diameter × 305 mm of length) were purchased from Alfa Aesar. All chemicals were directly used as received without further purification.

2.2. Electrochemical Measurements

All the electrochemical measurements were conducted using the electrochemical work stations (CHI440A (CH Instrument, Austin, Texas), and Autolab, PGSTAT100N) with a three-electrode system. A glassy carbon (GC, 3 mm of diameter) and graphite rod GR (supplied from Goodfellow, 3 mm diameter) were used as working electrode. Silver chloride electrode (Ag/AgCl, saturated KCl/AgCl solution), and graphite rod were used as the reference and the counter electrodes, respectively. The electrolytes (0.5 M H_2SO_4) were continuously deaerated using highly purified Argon bubbles for 30 minutes before the electrochemical tests. During the experiments, all the electrolytes were always kept under an inert atmosphere. The linear sweep voltammetry (LSV) with a scan rate of 5 mV/s was used for the hydrogen evolution reaction test. The LSV curves are corrected through the ohmic potential drop utilizing IR compensation test. The double-layer capacitance was evaluated by cyclic voltammetry (CV) with the different scan rates (10 mV/s, 20 mV/s, 40 mV/s, 60 mV/s, and 100 mV/s) in a non-faradaic region. The electrochemical impedance spectroscopy (EIS) was collected by Autolab with the frequency range of 100 kHz to 0.1 Hz at the AC amplitude of 10 mV. All the potentials were converted to reversible hydrogen electrode (RHE) according to the equation:

$$E(V/RHE) = E(V/Ag/AgCl) + 0.197 + 0.0592 \times pH$$

2.3. Preparation of platinum/graphite rod (Pt/GR)

First, the polished and cleaned GR electrode materials were put into the 0.1 M LiTFSI in ACN dry organic solvent, 1 cm of length was immersed. Then, a suitable voltage was applied by a means of chronoamperometry (CA) at the GR electrode. Next, the cathodically activated GR (A-GR) electrode with self-reducing power was rinsed by ACN, and quickly immersed into 1.25 mM K_2PtCl_4 aqueous solution to reduce the platinum. Finally, the Pt/Li-GR electrocatalyst sample was obtained after rinsing and drying. Similarly, Pt/Na-GR and Pt/K-GR were prepared after the cathodic activation of GR in in ACN solvent containing 0.1 M $NaBF_4$ and 0.1 M KBF_4, respectively.

For commercial Pt/C ink, 1 mg of Pt supported on graphitized carbon (Pt/C 20 wt.% loading), was dispersed in 20 µL of 5 wt % Nafion and 380 µL of absolute ethanol under sonication for 3 times 10 minutes. Then 10 µL of the homogeneous catalyst ink was dropwise added onto the surface of a GC or GR electrode and naturally dried at room temperature. The samples were labeled as Pt/C/GC and Pt/C/GR, respectively.

2.4. Characterization

The electrochemical measurements were applied using the CHI440A (CH Instrument, Austin, Texas) and Autolab (PGSTAT 100N) electrochemical work stations. The morphology of the as-prepared electrode materials was recorded by scanning electron microscope (SEM, Zeiss SUPRA 40) and elemental mapping was obtained by energy-dispersive X-ray spectroscopy (EDS). The XPS investigations were achieved using a Thermo VG Scientific ESCALAB 250 system with a monochromatic Al kα ($h\upsilon$ = 1486.6 eV). For the survey and the high resolution spectra the used pass energy was 100 and 40 eV, respectively. Data acquisition and processing were performed using the Avantage software. Spectral calibration was determined by setting the main C(1s) component at 285 eV. Atomic percentages have been determined using the software and taking into account photoemission cross sections, analyzer transmission, and variation of electron mean free paths with kinetic energy. Raman spectra were recorded at room temperature using a triple spectrometer Jobin Yvon T64000 and a LABRAM HR spectrometer with a solid-state laser (λ = 633 nm).

3. Results and discussion

Scheme 1 summarizes the used synthetic strategy for generating metal supported graphite rod. Precisely, graphite was electrochemically reduced in organic dry solution containing alkali metal salts as electrolyte. This process leads to generate a new phase [$C^{\delta-}$, $A^{\gamma+}$] owning a reducing power that is further used to

spontaneously reduce metallic salts (i.e $PtCl_4^{2-}$ and $PdCl_4^{2-}$) and subsequently generating Pt or Pd particles supported graphite materials.

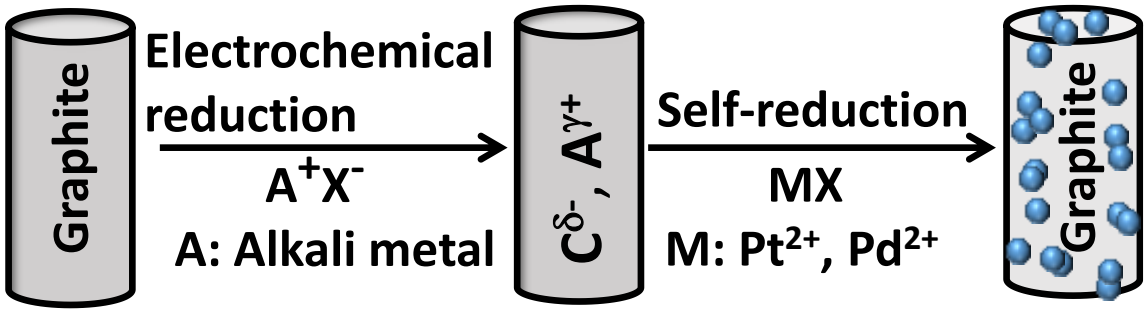

Scheme 1. Illustration of the fabrication of metal supported graphite electrode.

The cathodic activation of graphite rod (GR) was performed in dry acetonitrile (ACN) solution containing 0.1 M LiTFSI as electrolyte. The GR was polarized at negative potential –2.4 V vs Ag/AgCl during 60 s and the recorded chronoamperometry is shown in Fig. 1a (the resulting sample is labeled A-GR). During the electrochemical polarization the injected charge was about –0.129 $C.cm^{-2}$ attributed to the electrochemical reduction of graphite to generate new phase with a general formula [C_n^-, Li^+, LiTFSI] [39,40].

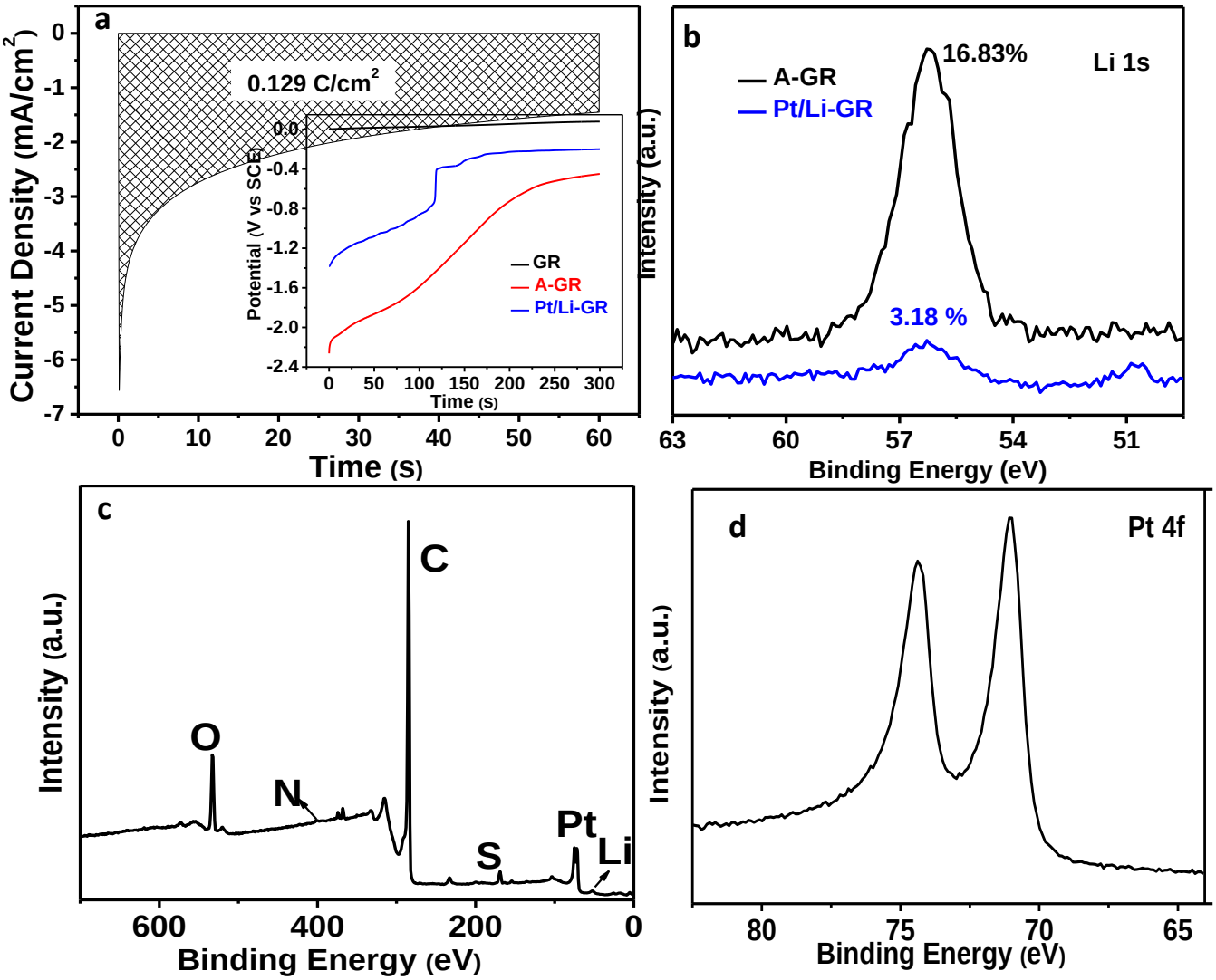

Fig. 1. (a) Chronaoamperometry curve of GR at –2.4 V vs. SCE in 0.1 M LiTFSI ACN during 60 s, (inset: OCP curves of GR and A-GR in 0.1 M LiTFSI ACN, and Pt/Li-GR in 1.25 mM K_2PtCl_4 aqueous solution). (b) High resolution XPS spectra of A-GR and Pt/Li-GR for Li 1s element. (c) XPS survey spectrum of Pt/Li-GR. (d) High resolution XPS spectra of Pt/Li-GR for Pt 4f.

Next, the open circuit potentials (OCP) (inset Fig. 1) were measured for the GR (black curve) and for the electrochemically activated GR (A-GR, red curve) in ACN electrolytic solution. Compared to GR the A-GR displays a negative OCP close to –2.1 V. The latter reach –1.8 V after 100 s and a plateau at –0.6 V after 250 s. This result confirms the high reducing power of the A-GR which could be used in self-reducing process. In another experiment, the freshly A-GR was immersed in aqueous solution containing K_2PtCl_4, the corresponding OCP curve (blue curve) displays initial OCP value at –1.4 V followed by continuous potential increases to –0.75 V during 120 s, next, an abrupt potential jump to –0.3 V is observed followed

by a plateau. The change in the OCP behaves like a discharge curve and is attributed to the loss of the injected charge due to the reduction of Pt^{2+} to Pt and also H^+ reduction as attested by the presence of H_2 bubble.

To accurately investigate the chemical compositions of A-GR and Pt/Li-GR electrodes, X-ray photoelectron spectroscopy (XPS) is conducted. Fig. 1b shows the XPS spectra of Li 1s recorded on A-GR (black line) and Pt/Li-GR (blue line). For A-GR electrode the XPS shows a peak at 56 eV attributed to Li 1s suggesting the presence of Li^+ on the GR surface. Deeper analysis exhibits that the lithium atomic percentage is 16.83% and that of sulfur (TFSI anion) is around 2.08%. One has to note that the expected theoretical atomic ratio of Li/S is 0.5 (Fig. S1) while the experimental ratio (Li/S) is around 8. This difference confirms the intercalation of Li^+ ions [43]. For Pt/Li-GR the XPS survey spectrum (Fig. 1c) shows as expected the presence of Li, S, C, N, O and Pt elements. The XPS survey spectrum displays a background increases after the Li 1s signal; this effect is due to the electron scattering confirming the intercalation of Li^+ into the GR. Compared to freshly A-GR the atomic percentage of Li 1s decreases to 3.1% suggesting Li^+ loss during the self-reduction process. The XPS spectrum of Pt 4f (Fig. 1d) displays the presence of intensive doublet at 71 and 74.5 eV attributed to metallic Pt. Similarly, the background increases after the Pt signal (Fig. 1c) suggests the presence of Pt inside the GR. The atomic percentage of the Pt in the investigated sample was found to be around 0.8% suggesting a low Pt mass loading compared to commercial Pt/C 20 wt%. In addition, the XRD patterns of the GR, activated GR and Pt/Li-GR samples display exclusively peaks patterns originated from the GR sample (Fig. S2a). The absence of characteristic Pt peaks in the sample Pt/Li-GR is probably due to the low Pt mass loading in the generated Pt/Li-GR sample. In the literature, F. Hutagalung et al reported that the Pt XRD peaks are not visible for a Pt supported carbon with a metal loading below 1 wt% [44]. Besides, Raman spectroscopy is a convenient method for investigating insertion materials process [45]. As expected, the Raman spectrum recorded on GR sample shows the presence of three characteristics peaks located at 1335 cm^{-1}, 1582 cm^{-1} and 2665 cm^{-1} attributed to the D, G and 2D bands, respectively [46] (Fig. S2b). The Raman spectra for A-GR and Pt/Li-GR shows the same peaks however a shift of the characteristics bands by 5 to 10 cm^{-1} is observed for the G and 2D bands, respectively. The Raman shift of the G and 2D bands has been attributed to the occurrence of intercalation process into graphite and/or to the charges transfer between the Pt particles and the graphite [46, 47].

Surface investigations were complemented by recording the scanning electron microscope (SEM) images of Pt/Li-GR electrode. Fig. 2a, and S3 display the presence of bright areas that correspond to Pt particles

with a diameter distribution ranged from 10 to 50 nm anchored onto the graphite areas. In addition compared to GR, the Pt/Li-GR image shows the presence of graphite swelling confirming that the GR reduction induces a morphological change of the electrode surfaces as previously reported [33]. Fig. 2b shows the EDS image confirming the presence of Pt supported onto GR electrode and indicating the uniform distributions of Pt nanoparticles on the surface.

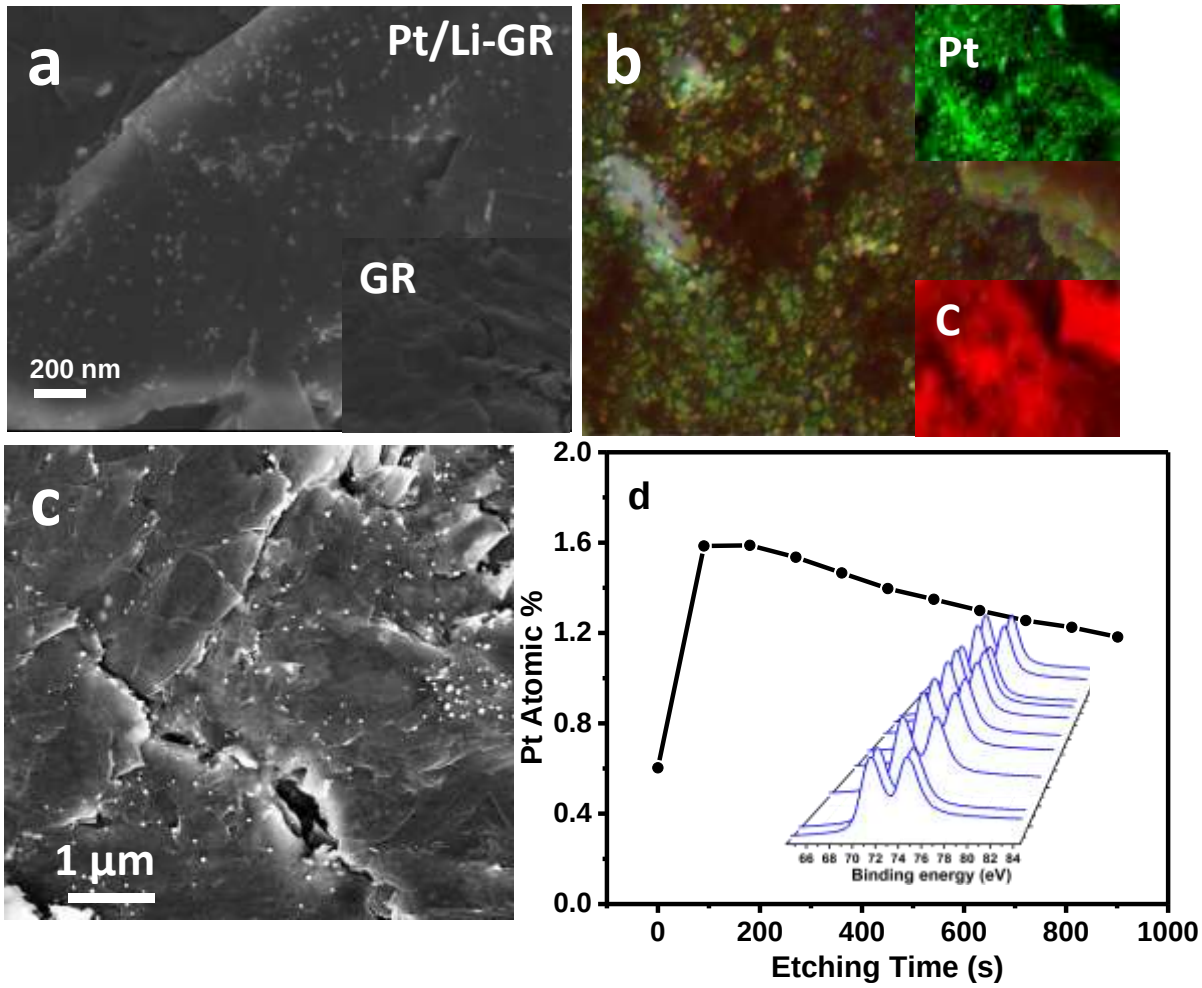

Fig. 2. (a) SEM image of Pt/Li-GR, (b) the corresponding SEM-EDX elemental mapping of Pt/Li-GR. (c) SEM image inside the Pt/Li-GR after removal of 200 µm. (d) Variation of the atomic% of Pt 4f as function of the etching time, (inset the XPS spectrum of Pt 4f of Pt/Li-GR after successive ablation).

To further confirm the presence of Pt inside the generated Pt/Li-GR electrode, the SEM image was recorded after removing 200 µm of the extreme surface. The recorded SEM image, Fig. 2c, shows bright areas corresponding to Pt particles, demonstrating that Pt nanoparticles decorate not only the surface but also inside the GR. In addition, XPS investigations using etching process was performed.

Fig. 2d shows the variation of the atomic percentage of Pt as function of the etching time. During the first 100 s etching the %Pt increases from 0.6% to 1.6%. After that, the %Pt decreases slightly but still higher than the initial value despite the continuous etching process. Besides, the O and the Li atomic percentages are lost after 50 s etching process. Additionally, the presence of Pt in Pt/Li-GR was also proved by recording cyclic voltammetry (CV) with a scan rate of 50 mV/s in 0.5 M H_2SO_4 electrolyte solution (Fig. S4). The recorded CV shows the presence of reduction and oxidation peaks characteristic of the adsorption and desorption of H atoms at the Pt surface. Overall, these results confirm the spontaneous growth of Pt onto and/or into activated GR. The spontaneous reduction of Pt^{2+} occurs, similarly to our previously reported works [38,41], following the reaction: $[C_n^-, Li^+,] + Pt^{2+} \rightarrow [C] + Pt + Li^+$

The electrocatalytic HER performance of the generated Pt/Li-GR electrocatalysts was evaluated in an Ar-saturated 0.5 M H_2SO_4 solution. Fig. 3a shows the linear sweep voltammetry, LSV, of Pt/Li-GR as well as the LSV recorded with benchmark Pt/C ink catalyst supported on GR and glassy carbon (GC).

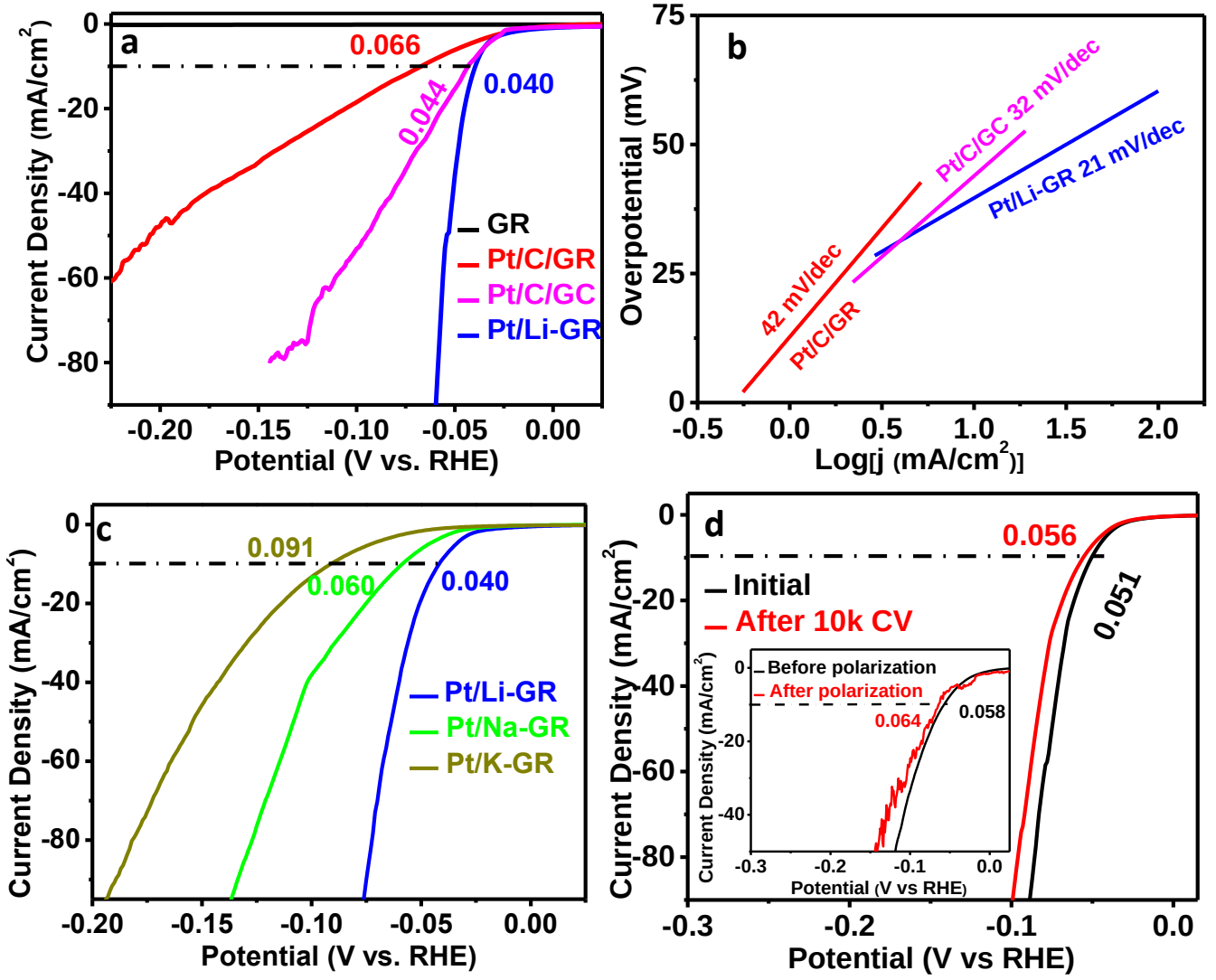

Fig. 3. (a) LSV's polarization curves of GR, Pt/Li-GR, and commercial Pt/C supported on GC and on GR in 0.5 H_2SO_4 solution, (b) Tafel plots derived from the LSV's curves. (c) LSV's polarization curves of Pt/Li-GR, Pt/Na-GR and Pt/K-GR. (d) LSV curves of Pt/Li-GR before and after 10K cycles CV test, inset LSV curves of Pt/Li-GR before and after chronopotentiometric test.

The Pt/Li-GR displays pronounced HER activity as attested by a low onset potential and higher current density at low overpotential (Table S1). An overpotential of 40 mV is needed to reach a current density of 10 $mA.cm^{-2}$. This value is lower than that observed for commercial Pt/C catalyst supported on GC (44 mV) or on GR (66 mV). Interestingly, for a higher current density of 50 $mA.cm^{-2}$ the needed overpotential is only 52 mV for the Pt/Li-GR while an overpotential about 100 and 204 mV is required for the Pt/C/GC and Pt/C/GR, respectively. This result confirms that the electrochemical activation of graphite followed by the spontaneous reduction generates Pt supported graphite with a higher performance compared to the state of the art Pt/C catalyst. One has to note, that only small deviation of the overpotential (±10 mV) @10 $mA.cm^{-2}$ is observed for different freshly prepared Pt/Li-GR electrodes. Besides that, other parameters control the performance of the as-prepared electrocatalyst including the injected charge during the reductive activation and the immersion times during the self-reduction process in aqueous solution containing K_2PtCl_4. The optimum parameters for Pt/Li-GR electrocatalyst are a cathodic activation at −2.4 V vs. SCE for 60 s and spontaneous reduction for 180 s (Fig. S5, S6, and Table S2). Figure S7 shows the comparison of the LSV curves recoded with and without IR compensation demonstrating that the compensation affects similarly the investigated materials. In another experiment, the LSV recorded on Pt electrode and Pt electrochemically deposited onto graphite rod (Pt/GR) are shown in Fig. S8. Both electrodes show an overpotential value of 83 and 140 mV to reach the 10 $mA.cm^{-2}$ for Pt and Pt/GR, respectively. These electrodes display lower performances than that recorded using the activated graphite approach to generate the Pt/Li-GR catalyst.

Besides, HER kinetics of the catalysts was investigated using Tafel analysis. Fig. 3c shows the Tafel plots derived from the LSV curves. The Pt/Li-GR shows a small Tafel slope value of 21 $mV.dec^{-1}$ suggesting the Tafel step as the rate-determining step, i.e., the Volmer–Tafel mechanism. This value is lower than that observed with Pt/C/GR (42 $mV.dec^{-1}$), and Pt/C/GC (32 $mV.dec^{-1}$) and clearly confirm the presence of a faster HER kinetics on Pt/Li-GR catalyst.

To investigate the intrinsic charge-transfer kinetics of Pt/Li-GR electrocatalysts, the EIS measurements were conducted (Fig. S9). The charge transfer resistance (R_{CT}) of the Pt/Li-GR was found to be close to that recorded on Pt/C/GC suggesting favorable charge transfer (Fig. S9a). In addition, the fitted charge-transfer resistance (R_{CT}) values of Pt/Li-GR electrocatalysts for different overpotential 60 mV, 100 mV,

300 mV, and 500 mV are found to be 26, 21, 17, and 5 Ω, respectively (Fig S9b). The results show that the R_{CT} decreases with the increases of overpotential value suggesting a higher charge transfer of the electrocatalytic reaction on the catalyst surface [48]. Moreover, compared to commercial Pt/C catalyst, Pt/Li-GR displays lower charge transfer resistance suggesting faster electron transfer and contact between the Pt and the GR. Furthermore, the electrochemical double-layer capacitance (C_{dl}) was used to evaluate the electrochemically active surface area of electrocatalysts, which was collected by the CV curves recorded at different low scan rates in the capacitive region [49]. The value measured for Pt/Li-GR is 2.44 $mF.cm^{-2}$ which is higher than that of Pt/C/GC (1.36 $mF.cm^{-2}$) and Pt/C/GR (0.57 $mF.cm^{-2}$) shown in TableS1. It is well known that the change of the C_{dl} is linked to the active surface area. The increase of the C_{dl} for Pt/Li-GR electrode is probably due to the swelling of the graphite during the cathodic activation as well as the proliferation of the Pt active sites onto and inside the GR. Thus, the higher C_{dl} value for Pt/Li-GR suggests a high exposure of active sites and as consequence a higher HER activity. The electrochemical active surface area (ECSA) could be estimated from the C_{dl} divided by the specific capacitance (40 $\mu F.cm^{-2}$). The Pt/Li-GR gives a value about 60 which is found to be twice the value obtained for Pt/C/GC and almost five times higher than that for Pt/C/GR (Table S1).

To investigate the role of the supporting electrolyte cation, the cathodic activation was performed using various alkali metal salts, namely $NaBF_4$ and KBF_4. After the cathodic activation, the as-prepared GR were immersed into aqueous K_2PtCl_4 solution leading to the formation of Pt/alkali metal-GR electrodes. Fig. 3c compares the LSV's polarization curves recorded for Pt/Li-GR, Pt/Na-GR and Pt/K-GR. All the electrodes display pronounced HER activity as attested by a low onset potential and higher current density at low overpotential. This first result confirms that the cathodic activation followed by self-reduction is a successful method for generating Pt supported GR catalyst. The close comparison demonstrates that the activation in the presence of Li^+ provides a better electrocatalytic performance with 40 mV overpotential to reach a current density of 10 $mA.cm^{-2}$, while in the case of Na^+ and K^+ an overpotential about 60 and 91 mV is required, respectively. This tendency could be explained by the atomic radius of the alkali metal (i.e, $Li^+ < Na^+ < K^+$). Thus, for the smallest cation, it is expected that the intercalation processed more deeply onto GR and as consequence generating a higher electrocatalyst site.

Another important characteristic of the catalyst is the stability. The durability of the generated Pt/Li-GR catalysts was carried out by performing 10000 potential sweep between 0.7 and −0.2 V vs RHE. Fig. 3d compares the initial LSV polarization curve to that performed after CV cycling. The Pt/Li-GR catalyst displays a negligible increase of the overpotential η@10 $mA.cm^{-2}$ (5 mV) after 10000 cycles CV. In an-

other experiment, the durability of the same electrocatalyst is further investigated using chronopotentiometric method (a current density about 10 mA.cm^{-2} was applied during 13000 s). During the CP test shown in Fig. S10, almost negligible overpotential is observed with an average value around 60 mV overpotential. The LSV's curves, shown in the inset Fig. 3d, displays an overpotential (η@10 mA.cm^{-2}) about 64 mV displaying a small shifts about 6 mV after the polarization. In addition, the Pt/Li-GR electrocatalytic performance was tested before and after the lockdown in Paris (55 days) showing a negligible overpotential shift of about 8 mV. All, these results indicate the high electrochemical stability of the generated Pt/Li-GR catalyst. One has to note that unlike commercial Pt/C catalyst, all the electrocatalytic performances and stability tests were performed using the as-prepared Pt supported GR catalyst without adding a polymer binder (i.e. Nafion).

The preceding results indicate that Pt supported graphite catalysts, generated by the electrochemical activation approach, possesses excellent electrocatalytic activity and stability towards the HER. For this reason, further experiments were performed with the aim to demonstrate the generality of the proposed approach. Thus, similar experiments were performed to generate Pd supported electrochemically activated GR as electrocatalyst. Subsequent to the reductive activation of GR in LiTFSI electrolytic solution, the A-GR was immersed in aqueous solution containing Na_2PCl_4 salt. The SEM image of the generated Pd/Li-GR shows the presence of Pd particles supported on graphite as well as the swelling of the graphite (Fig. 4a). The Pd particles size is ranged from 10 to 30 nm.

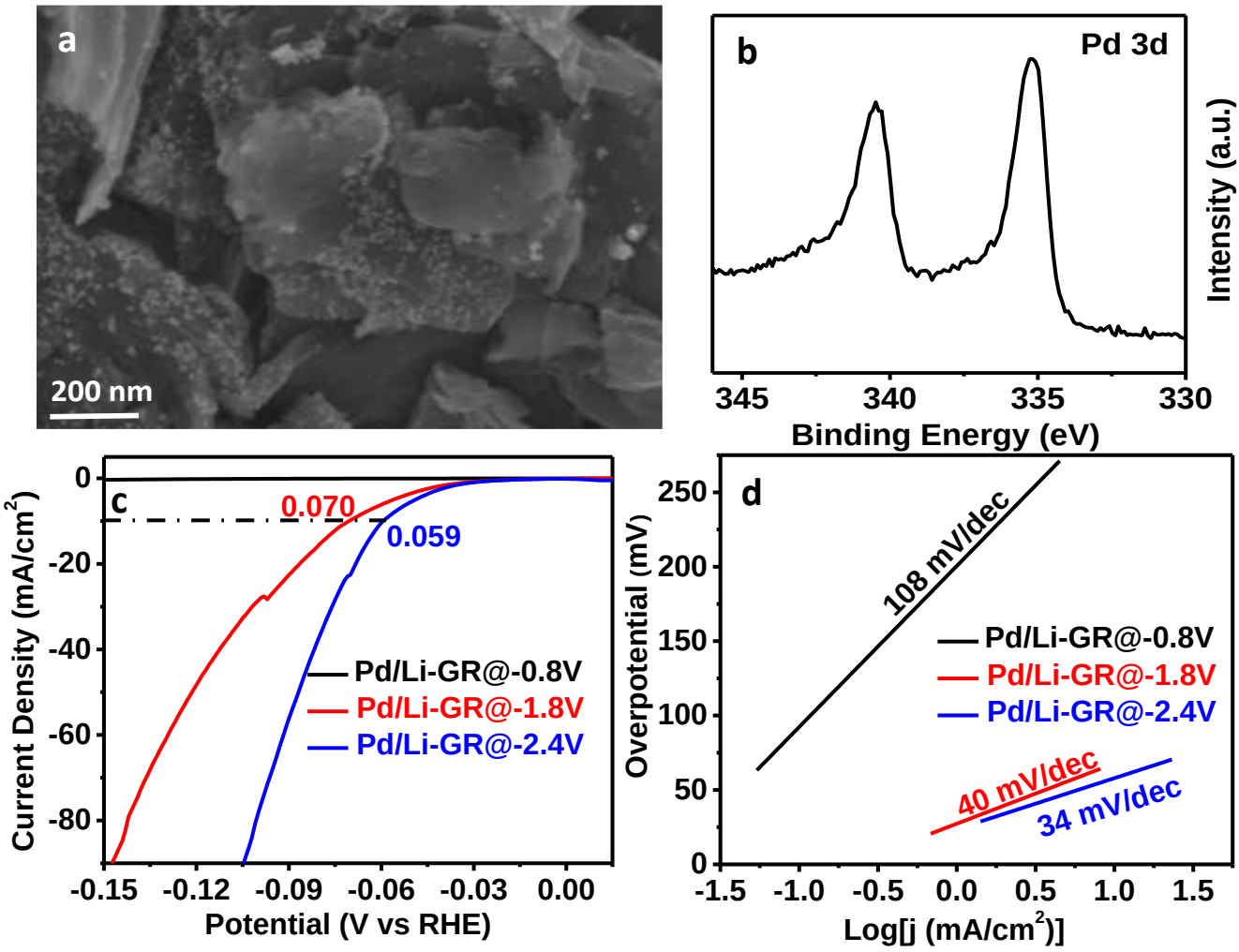

Fig. 4. (a) SEM image of Pd/Li-GR, (b) XPS high resolution spectrum of Pd/Li-GR for Pd 3d, (c) LSV's polarization curves of Pd/Li-GR as-prepared by electrochemical activation at –0.8 V, −1.8 V and −2.4 V vs SCE, respectively. (d) Tafel plots derived from the LSV's curves.

In addition, the XPS spectrum of Pd 3d (Fig. 4b) displays the presence of intensive doublet at 335.2 and 340.5 eV attributed to metallic Pd. Similar to the case of Pt/Li-GR, in the survey spectrum the background increases after the Pd signal suggesting the presence of this element onto and inside the GR. These results confirm the formation of Pd nanoparticles supported GR after the cathodic activation followed by self-reduction.

Furthermore, the electrocatalytic activity of the Pd/Li-GR was investigated and the results are summarized in Fig. 4c. The LSV's polarization curves show that the HER activity starts to be visible for Pd/Li-GR activated at −1.8 V. The Pd/Li-GR@−2.4 V electrocatalyst displays the best activity for HER than that of Pd/Li-GR@−0.8 V and Pd/Li-GR@−1.8 V catalysts. It is worth noting that the required overpotential of

Pd/Li-GR@−2.4 V to reach a current density of 10 mA.cm^{-2} is 59 mV. This value is lower than that of 20 wt% Pd/C (170 mV), 30 wt% Pd/C (96 mV), and pure Pd nanoparticles (181 mV) [50,51]. The Tafel plot analysis shows that the Pd/GR@−2.4 V electrocatalyst exhibits a Tafel slope value of 34 mV.dec^{-1} suggesting the Tafel step as the rate-determining step as well as the presence of a faster HER kinetics. Interestingly, the observed Tafel slope is almost similar to that recorded on commercial Pt/C catalyst. These results prove that the cathodic activation could be commonly used as an easy approach to generate metal supported graphite catalysts for an efficient HER.

4. Conclusion

In summary, we present a facile and effective pathway to fabricate metal supported GR electrocatalysts. The cathodically activated GR materials were used as spontaneous reductant to reduce Pt or Pd metallic salts at room temperature. The SEM images and XPS results consistently agree with the fact that the Pt nanoparticles were successfully anchored on and into the GR. In addition, the prepared Pt/Li-GR electrocatalysts reveal an impressive performance and stability toward HER comparable to that recorded on commercial Pt/C. Furthermore, our strategy can be easily extended to the synthesis of other metal/graphite electrocatalysts with higher HER activity as demonstrated for Pd/Li-GR. The latter outperforms the benchmark Pd/C catalyst and shows almost comparable HER activity as the state of the art Pt/C catalyst. This research provides an original approach to generate metallic nanoparticles supported graphite. We anticipate that the proposed approach could be extended to various metals and electrode materials as well as a potential use for other electrocatalytic reactions.

ASSOCIATED CONTENT

AUTHOR INFORMATION

Corresponding Author *E-mail: jalal.ghilane@u-paris.fr

ORCID: 0000-0002-8792-6337

Notes

The authors declare no competing financial interests.

Author Contributions

The manuscript was written through contributions of all authors. All authors have given approval to the final version of the manuscript.

ACKNOWLEDGMENT

We thank the support from the CNRS and doctoral school (ED388) and thank Dr. Sarra Gam Derouich (for performing the EDS mapping), Dr. Philippe Decorse (for the XPS analysis). H.-Z. Yu thanks China Scholarship Council for financial support (File No. 201906950024).

REFERENCES

[1] Z.W. Seh, J. Kibsgaard, C.F. Dickens, I. Chorkendorff, J.K. Norskov, T.F. Jaramillo, Combining theory and experiment in electrocatalysis: Insights into materials design. Science 355 (2017), 6321.

[2] H.Z. Yu, Y. Wang, J. Ying, S.M. Wu, Y. Lu, J. Hu, J.S. Hu, L. Shen, Y.X. Xiao, W. Geng, G.G. Chang, C. Janiak, W.H. Li, X.Y. Yang, Hydrogen evolution enhancement over a cobalt-based schottky interface. ACS Appl. Mater. Interfaces 11 (2019), 27641–27647.

[3] J. Ying, G.P. Jiang, Z.P. Cano, L. Han, X.Y. Yang, Z.W. Chen, Nitrogen-doped hollow porous carbon polyhedrons embedded with highly dispersed Pt nanoparticles as a highly efficient and stable hydrogen evolution electrocatalyst. Nano Energy 40(2017), 88–94.

[4] M. Tahir, L. He, W. Yang, X. Hong, W.A. Haider, H. Tang, Z. Zhu, K.A. Owusu, L. Mai, Boosting the electrochemical performance and reliability of conducting polymer microelectrode via intermediate graphene for on-chip asymmetric micro-supercapacitor. J. Energy Chem. 49 (2020), 224–232.

[5] K.R.G. Lim, A.D. Handoko, S.K. Nemani, B. Wyatt, H.Y. Jiang, J. Tang, B. Anasori, Z.W. She, Rational De-sign of Two-Dimensional Transition Metal Carbide/Nitride (MXene) Hybrids and Nanocomposites for Catalytic Energy Storage and Conversion. ACS Nano 14 (2020), 10834–10864.

[6] T.T. Yang, T.L. Tan, W.A. Saidi, High activity toward the hydrogen evolution reaction on the edges of MoS2-supported platinum nanoclusters using cluster expansion and electrochemical modeling. Chem. Mater. 32 (2020), 1315–1321.

[7] C. Wei, R.R. Rao, J. Peng, B. Huang, I.E.L. Stephens, M. Risch, Z.J. Xu, Y. Shao-Horn, Recommended practices and benchmark activity for hydrogen and oxygen electrocatalysis in water splitting and fuel cells. Adv. Mater. 31 (2019), e1806296.

[8] J. Diao, Y. Qiu, S. Liu, W. Wang, K. Chen, H. Li, W. Yuan, Y. Qu, X. Guo, Interfacial engineering of W_2N/WC heterostructures derived from solid-state synthesis: A highly efficient trifunctional electrocatalyst for ORR, OER, and HER. Adv. Mater. 32 (2020), e1905679.

[9] Y. Yang, H. Yao, Z. Yu, S.M. Islam, H. He, M. Yuan, Y. Yue, K. Xu, W. Hao, G. Sun, H. Li, S. Ma, P. Zapol, M.G. Kanatzidis, Hierarchical nanoassembly of MoS_2/Co_9S_8/Ni_3S_2/Ni as a highly efficient electrocatalyst for overall water splitting in a wide pH range. J. Am. Chem. Soc. 141 (2019), 10417–10430.

[10] T. Rajala, R. Kronberg, R. Backhouse, M.E.M. Buan, M. Tripathi, A. Zitolo, H. Jiang, K. Laasonen, T. Susi, F. Jaouen, T. Kallio, A platinum nanowire electrocatalyst on single-walled carbon nanotubes to drive hydrogen evolution. Appl. Catal. B: Environ 265 (2020), 118582.

[11] H. Zhang, X. Yang, H. Zhang, J. Ma, Z. Huang, J. Li, Y. Wang, Transition-Metal Carbides as Hydrogen Evolution Reduction Electrocatalysts: Synthetic Methods and Optimization Strategies. Chem. Eur. J. 27 (2021), 5074–5090.

[12] C. Hu, Q. Dai, L. Dai, Multifunctional carbon-based metal-free catalysts for advanced energy conversion and storage. Cell Rep. Phys. Sci. 2 (2021), 100328.

[13] D. Wu, K. Kusada, T. Yamamoto, T. Toriyama, S. Matsu-mura, I. Gueye, O. Seo, J. Kim, S. Hiroi, O. Sakata, S. Kawaguchi, Y. Kubota, H. Kitagawa, On the electronic structure and hydrogen evolution reaction activity of platinum group metal-based high entropy alloy nanoparticles. Chem. Sci. 11 (2020), 12731–12736.

[14] R.Q. Yao, Y.T. Zhou, H. Shi, Q.H. Zhang, L. Gu, Z. Wen, X.Y. Lang, Q. Jiang, Nanoporous palladium–silver surface alloys as efficient and pH-universal catalysts for the hydrogen evolution reaction. ACS Energy Lett. 4 (2019), 1379–1386.

[15] M.P. Browne, F. Novotný, D. Bousa, Z. Sofer, M. Pumera, Flexible Pt/graphene foil containing only 6.6 wt% of Pt has a comparable hydrogen evolution reaction performance to platinum metal. ACS Sustainable Chem. Eng. 7 (2019), 11721–11727.

[16] C. Xie, Z. Niu, D. Kim, M. Li, P. Yang, Surface and interface control in nanoparticle catalysis. Chem. Rev. 120 (2020), 1184–1249.

[17] K. Ding, D.A. Cullen, L. Zhang, Z. Cao, A.D. Roy, I.N. Ivanov, D. Cao, A general synthesis approach for supported bimetallic nanoparticles via surface inorganometalic chemistry. Science 362 (2018), 560–564.

[18] J. Kim, H. Kim, Lee, J. W. B. Ruqia, H. Baik, H.S. Oh, S.M. Paek, H.K. Lim, C.H. Choi, S.I. Choi, Theoretical and experimental understanding of hydrogen evolution reaction kinetics in alkaline electrolytes with Pt-based core–shell nanocrystals. J. Am. Chem. Soc. 141 (2019), 18256–18263.

[19] Z.Y. Zhou, N. Tian, J.T. Li, I. Broadwell, S.G. Sun, Nanomaterials of high surface energy with exceptional properties in catalysis and energy storage. Chem. Soc. Rev. 40 (2011), 4167–4185.

[20] H. Jin, X. Liu, S. Chen, A. Vasileff, L. Li, Y. Jiao, L. Song, Y. Zheng, S.Z. Qiao, Heteroatom-Doped Transition Metal Electrocatalysts for Hydrogen Evolution Reaction. ACS Energy Lett. 4 (2019), 805–810.

[21] H. Song, Y. Li, L. Shang, Z. Tang, T. Zhang, S. Lu, De-signed controllable nitrogen-doped carbon-dots-loaded MoP nanoparticles for boosting hydrogen evolution reaction in alkaline medium. Nano Energy 72 (2020), 104730.

[22] J. Zhu, L. Hu, P. Zhao, L.Y.S. Lee, K.Y. Wong, Recent Advances in Electrocatalytic Hydrogen Evolution Using Nanoparticles. Chem. Rev. 120 (2020), 851–918.

[23] S.M. El-Refaei, P.A. Russo, N. Pinna, Recent Advances in Multi-metal and Doped Transition-Metal Phosphides for the Hydrogen Evolution Reaction at Different pH values. ACS App. Mater. Interfaces 13 (2021), 22077–22097.

[24] P. Trogadas, T.F. Fuller, P. Strasser, Carbon as catalyst and support for electrochemical energy conversion. Carbon 75 (2014), 5–42.

[25] I.C. Gerber, P. Serp, A theory/experience description of support effects in carbon-supported catalysts. Chem. Rev. 120 (2020), 1250–1349.

[26] S. Ott, A. Orfanidi, H. Schmies, B. Anke, H.N. Nong, J. Hubner, U. Gernert, M. Gliech, M. Lerch, P. Strasser, Ionomer distribution control in porous carbon-supported catalyst layers for high-power and low Pt-loaded proton exchange membrane fuel cells. Nat. Mater. 19 (2020), 77–85.

[27] J. Xu, R. Li, R. Zeng, X. Yan, Q. Zhao, J. Ba, W. Luo, D. Meng, Platinum Single Atoms Supported on Nanoarray-Structured Nitrogen-Doped Graphite Foil with Enhanced Catalytic Performance for Hydrogen Evolution Reaction. ACS Appl. Mater. Interfaces 12 (2020), 38106–38112.

[28] T.N. Pham-Truong, O. Mebarki, C. Ranjan, H. Randriamahazaka, J. Ghilane, Electrochemical growth of metallic nanoparticles onto immobilized polymer brush ionic liquid as a hybrid electrocatalyst for the hydrogen evolution reaction. ACS Appl. Mater. Interfaces 11 (2019), 38265–38275.

[29] S. Bencherif, M. Mechouet, J. Ghilane, Metallic nano-particles growth on ionic layer grafted onto glassy car-bon for hydrogen evolution reaction. J. Mol. Liq. 341 (2021), 117433.

[30] H.Z. Yu, S. Bencherif, T.N. Pham-Truong, J. Ghilane, Immobilization of molecule-based ionic liquids: a promising approach to improve elecrocatalyst performance towards the hydrogen evolution reaction. New J. Chem. 46 (2022), 454–464.

[31] D. Bélanger, J. Pinson, Electrografting: a powerful method for surface modification. Chem. Soc. Rev. 40 (2011), 3995–4048.

[32] C. Cougnon, J. Simonet, Cathodic reactivity of alkaline metal iodides toward platinum bulk. The formation of new reducing phases. Electrochem. Commun. 4 (2002), 266–271.

[33] C. Dano, J. Simonet, Cathodic reactivity of graphite with carbon dioxide: an efficient formation of carboxylated carbon materials. J. Electroanal. Chem. 564 (2004), 115–121.

[34] X. Feng, X. Sui, M.A. Hempenius, J. G. Vancso, Electrografting of Stimuli-Responsive, Redox Active Organometallic Polymers to Gold from Ionic Liquids. J. Am. Chem. Soc. 136 (2014), 7865–7868.

[35] J. Ghilane, O. Fontaine, P. Martin, J.C. Lacroix, Randriamahazaka, H. Formation of negative oxidation states of platinum and gold in redox ionic liquid: Electrochemical evidence. Electrochem. Commun. 10 (2008), 1205–1209.

[36] J. Ghilane, M. Guilloux-Viry, C. Lagrost, P. Hapiot, J. Simonet, Cathodic Modifications of Platinum Surfaces in Organic Solvent: Reversibility and Cation Type Effects. J. Phy. Chem. B 109 (2005), 14925–14931.

[37] J. Ghilane, M. Guilloux-Viry, C. Lagrost, J. Simonet, P. Hapiot, Reactivity of Platinum Metal with Organic Radical Anions from Metal to Negative Oxidation States. J. Am. Chem. Soc. 129 (2007), 6654–6661.

[38] S. Bouden, A. Dahi, F. Hauquier, H. Randriamahazaka, J. Ghilane, Multifunctional indium tin oxide electrode generated by unusual surface modification. Sci. Rep. 6 (2016), 36708.

[39] J.O. Besenhard, The electrochemical preparation and properties of ionic alkali metal-and NR4-graphite intercalation compounds in organic electrolytes. Carbon 14 (1976), 111–115.

[40] J. Simonet, H. Lund, Electrochemical behavior of graphite cathodes in the presence of tetraalkylammonium cations. J. Electroanal. Chem. 75 (1977), 719–730.

[41] J. Ghilane, J.C. Lacroix, Formation of a Bifunctional Redox System Using Electrochemical Reduction of Platinum in Ferrocene Based Ionic Liquid and Its Reactivity with Aryldiazonium. J. Am. Chem. Soc. 135 (2013), 4722–4728.

[42] J. Ghilane, M. Delamar, M. Guilloux-Viry, C. Lagrost, C. Mangeney, P. Hapiot, Indirect reduction of aryldiazonium salts onto cathodically activated platinum sur-faces: Formation of metal−organic structures. Langmuir 21 (2005), 6422–6429.

[43] J. Ghilane, C. Lagrost, M. Guilloux-Viry, J. Simonet, M. Delamar, C. Mangeney, P. Hapiot, Spectroscopic Evidence of Platinum Negative Oxidation States at Electrochemically Reduced Surfaces. J. Phys. Chem. C 111 (2007), 5701–5707.

[44] R. Siburian, M. M. Ali, K. Sebayang, M. Supeno, K. Tarigan, C. Simanjuntak, S. P. Aritonang, F. Hutagalung, The loading effect of Pt clusters on Pt/graphene nano sheets catalysts. Sci. Rep. (2021) 11:2532.

[45] R. Baddour-Hadjean, J.P. Pereira-Ramos, Raman Microspectrometry Applied to the Study of Electrode Materials for Lithium Batteries. Chem. Rev. 110 (2010), 1278—1319.

[46] C. Sole, N.E. Drewett, L.J. Hardwick, In situ Raman study of lithium-ion intercalation into microcrystalline graphite. Faraday Discuss. 172 (2014), 223—237.

[47] X. Zheng, W. Chen, G. Wang, Y. Yu, S. Qin, J. Fang, F. Wang, X.A. Zhang, The Raman redshift of graphene impacted by gold nanoparticles. AIP Adv. 5 (2015), 057133.

[48] D. Merki, H. Vrubel, L. Rovelli, S. Fierro, X. Hu, Fe, Co, and Ni ions promote the catalytic activity of amorphous molybdenum sulfide films for hydrogen evolution. Chem. Sci. 3 (2012), 2515–2525.

[49] S. Anantharaj, S. Noda, Appropriate use of electrochemical impedance spectroscopy in water splitting electrocatalysis. ChemElectroChem 7 (2020), 2297–2308.

[50] T. Bhowmik, M.K. Kundu, S. Barman, Palladium Nanoparticle–Graphitic Carbon Nitride Porous Synergistic Catalyst for Hydrogen Evolution/Oxidation Reactions over a Broad Range of pH and Correlation of Its Catalytic Activity with Measured Hydrogen Binding Energy. ACS Catal. 6 (2016), 1929–1941.

[51] R. Zhang, Z. Sun, R. Feng, Z. Lin, H. Liu, M. Li, Y. Yang, R. Shi, W. Zhang, Q. Chen, Rapid Adsorption Enables Interface Engineering of PdMnCo Alloy/Nitrogen-Doped Carbon as

Highly Efficient Electrocatalysts for Hydrogen Evolution Reaction. ACS Appl. Mater. Interfaces 9 (2017), 38419–38427.